Reynolds Number Effects on Boattail Drag of Wing-Bodies

David E. Reubush*
NASA Langley Research Center, Hampton, Va.

An investigation has been conducted in the Langley ⅓-m transonic cryogenic tunnel to determine the effects of varying Reynolds number on the boattail drag of wing-body configurations at subsonic speeds. Two boattailed cone-cylinder nacelle models were tested with a 60° delta wing at an angle of attack of 0°. Reynolds number, based on model length, was varied from about 2.5×10^6 to 67×10^6. Even though the presence of the wing had large effects on the boattail pressure coefficients, the results of this investigation were similar to those previously found for a series of isolated boattails. Boattail pressure coefficients in the expansion region became more negative with increasing Reynolds number, whereas those in the recompression region became more positive. These two effects were compensating, and, as a result, there was virtually no effect of Reynolds number on boattail pressure drag.

Nomenclature

A_m = maximum cross-sectional area of model
A_β = incremental area assigned to boattail static-pressure orifice for drag integration
C_D = drag coefficient
$C_{D,\beta}$ = boattail pressure drag coefficient, $\sum_{i=1}^{30 \text{ or } 50} C_{p,\beta,i}A_{\beta,i}/qA_m$
$C_{p,\beta}$ = boattail static pressure coefficients
d_m = maximum diameter of model
L = length of model from nose to beginning of boattail (characteristic length)
l = length of boattail
M = Mach number
M_∞ = freestream Mach number
p_t = freestream total pressure
q = freestream dynamic pressure
R = Reynolds number
T_t = freestream total temperature
x = axial distance aft from start of boattail
ϕ = meridian angle about model axis, clockwise positive facing upstream, 0° at top of model

Introduction

CURRENT prediction methods for full-scale aircraft propulsion system installation drag rely heavily on wind-tunnel simulation of the actual conditions. Wind-tunnel tests are required because the drag-producing components of the propulsion system usually are installed in areas where the flowfield is extremely complex; and, at present, there are no adequate theoretical techniques with which to predict these complex flows. Especially in the afterbody-nozzle region, high slopes and long boundary-layer runs result in large and unpredictable viscous effects on boattail pressure drag. Attention recently has been focused on scaling effects, particularly the effects of Reynolds number variation on boattail pressure drag. Investigations by NASA[1-5] have identified possible large effects of Reynolds number variation on installed boattail drag. In this work, flight tests were conducted utilizing an F-106 airplane that had two research nacelles mounted under the wings. The boattails to be tested were mounted on these nacelles, and the F-106 airplane was flown over a range of Reynolds numbers. The F-106 airplane in flight and a closeup of a typical boattail are shown in the upper left of Fig. 1. In addition to the flight tests, two scale models of the F-106 airplane were tested in a wind tunnel in order to obtain data at Reynolds numbers lower than those achievable in flight and to have a comparison between flight and wind-tunnel data. A typical result of boattail drag as a function of Reynolds number from one of these investigations is shown in the lower left of Fig. 1. These data imply that it would be impossible to extrapolate boattail drag data obtained in a wind tunnel to flight Reynolds numbers. These data have accentuated the need for further research in this area.

Until recently, the maximum Reynolds numbers achievable in wind tunnels were considerably lower than those achieved in flight; therefore, flight tests were the only means whereby data could be obtained over a significant Reynolds number range. However, the Langley Research Center has now in operation the ⅓-m transonic cryogenic tunnel.[6-12] This facility has the capability of operating at stagnation pressures from about 1 to 5 atm over a stagnation temperature range from about −320°F (78 K) to 170°F (350 K). As a result, substantial variations in Reynolds number can be obtained over the tunnel's operating Mach number range from about 0.1 to 1.2. The tunnel's operating Reynolds number envelopes for the investigations to be discussed herein are shown in the upper right of Fig. 1; the bars indicate the wind-tunnel flight-test range of the previous NASA work.

The unique capabilities of the cryogenic tunnel provide a ready means by which a single model can be tested over a large range of Reynolds numbers. With this capability available, a series of simple experiments was devised to develop a data base to provide an insight into the flow phenomena involved. The first experiment utilized a series of six isolated, sting-mounted, cone-cylinder nacelle models with four different boattail geometries (Fig. 2) which were tested in the cryogenic tunnel primarily at the subsonic Mach numbers of 0.6 and 0.9 at an angle of attack of 0°. Reynolds number based on the distance from the nose to the beginning of the boattail varied from about 2.5×10^6 to 106×10^6 at $M=0.6$ and varied from about 3.4×10^6 to 132×10^6 at $M=0.9$. Isolated boattails were tested to eliminate all extraneous effects and thereby isolate the pure effect of Reynolds number on boattail pressure drag. Results from this investigation have been reported previously in Ref. 13 and, therefore, will be summarized only briefly herein. The second experiment utilized two new models with nacelle and boattail geometries which duplicated two of the boattails from the isolated model test but with the provision to mount a delta wing on top of the nacelle in three positions (Figs. 3 and 4). These models were tested in the cryogenic tunnel primarily at the subsonic Mach

Presented as Paper 75-1294 at the AIAA/SAE 11th Propulsion Conference, Anaheim, Calif., Sept. 29-Oct. 1, 1975; submitted Sept. 29, 1975; revision received Jan. 20, 1977.

Index categories: Aerodynamics; Airbreathing Propulsion; Testing, Flight and Ground.

*Aerospace Engineer, High-Speed Aerodynamics Division. Member AIAA.

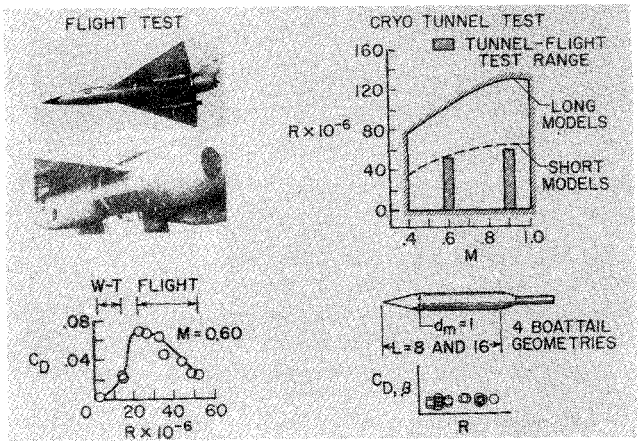

Fig. 1 Objective and scope of isolated boattail investigation.

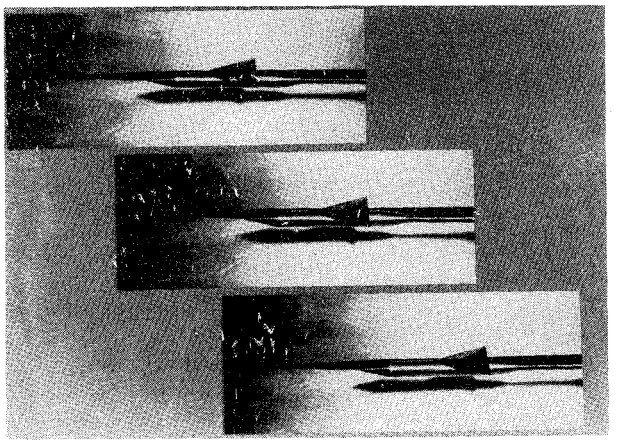

Fig. 3 Photograph of wing-body model showing three wing positions.

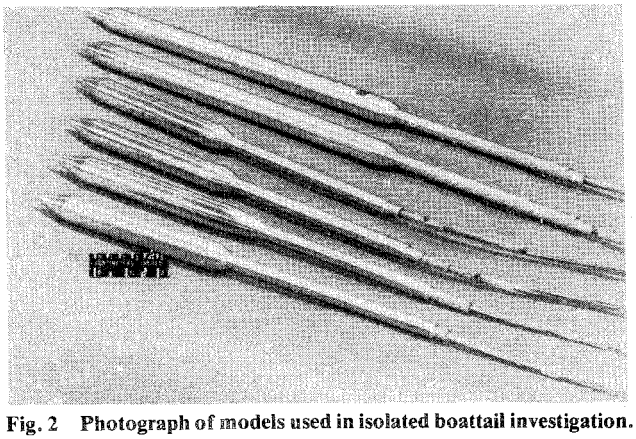

Fig. 2 Photograph of models used in isolated boattail investigation.

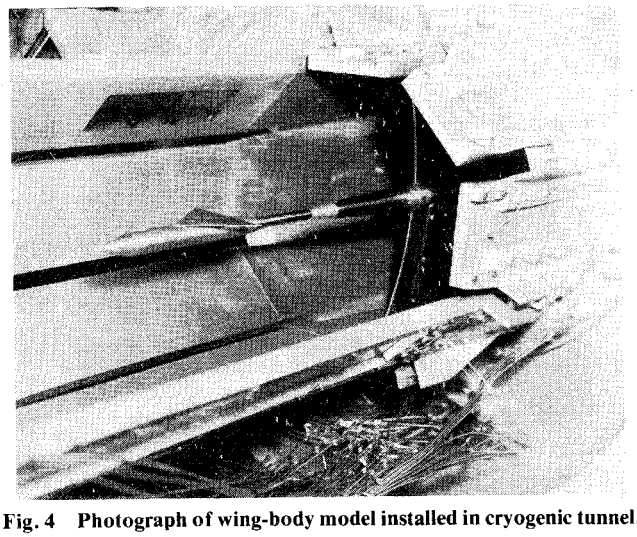

Fig. 4 Photograph of wing-body model installed in cryogenic tunnel.

numbers of 0.6, 0.85, and 0.9 at an angle of attack of 0°. Reynolds number based on the distance from the nose to the beginning of the boattail varied from about 2.5×10^6 to 57×10^6 at $M=0.6$, 3.5×10^6 to 67.5×10^6 at $M=0.85$, and $3.5\times^6$ to 68×10^6 at $M=0.9$. These models were tested to determine what effect, if any, Reynolds number has on the boattail drag of a simple wing-body configuration. The main purpose of this paper is to describe and discuss the results of this investigation.

Experimental Methods

The models used in the isolated boattail investigation are shown in Fig. 2. There was a total of six models: four short models of differing boattail geometry with a length of 8 in. (20.32 cm) from the nose to the start of the boattail (characteristic length), and two long models with a length of 16 in. (40.64 cm) from the nose to the start of the boattail. The boattail geometry of the two long models duplicated the boattail geometry of two of the short models. The four boattail geometries were circular arc with a length-to-maximum-diameter ratio (fineness ratio l/d_m) of 0.8, circular arc with a fineness ratio of 1.77, circular arc-conic with a fineness ratio of 0.96, and contoured with a fineness ratio of 0.95. It should be noted that the two circular arc boattails were scale models of two that have been tested in the Langley 16-ft transonic tunnel,[14] and the circular arc-conic and the contoured boattails were isolated scale models of two that have been wind-tunnel tested in the Lewis 8-×6-ft supersonic wind tunnel and flight tested on the F-106.[1-5]

The models all were sting mounted, with the diameter of the sting being equal to the model base diameter. Thus, the sting simulated the geometry of a jet exhaust plume for a nozzle operating at its design point.[14] The two circular arc boattails and the circular arc-conic boattail had sting-to-maximum-diameter ratios of 0.5, whereas the contoured had a sting-diameter-to-maximum-diameter ratio of 0.544. The length of the constant-diameter portion of the stings was such that, based on the work of Cahn[15] there should be no effect of the sting flare on the boattail pressure distributions.

The models were constructed of cast aluminum, with stainless-steel pressure tubes cast as an integral part of the model. The tubes were placed in the sand mold in the proper position, the aluminum poured, and the model machined to the proper contours. Each of the models was instrumented with 30 pressure orifices in three rows of 10 orifices each. Although it would have been desirable to have all of the orifices in one row, the fact that the models were only 1 in. (2.54 cm) in diameter combined with the number of orifices precluded this possibility.

The models used in the wing-body investigation duplicated the nacelle and boattail geometry of two of the short (8-in., 20.32-cm) isolated boattails: the $l/d_m=1.77$ circular arc boattail and the $l/d_m=0.96$ circular arc-conic boattail. These two were chosen because the former had all attached flow at all test Mach numbers, whereas the latter had some separated flow at all test Mach numbers. Construction of these models was slightly different from that of the isolated boattails in that a stainless-steel sting was used and the model cast around the sting and pressure tubes. By utilizing this method of construction, it was possible to instrument these models with 50 pressure orifices in five rows of 10 orifices each ($\phi=0°$, 45°, 135°, 180°, and 270°). Provision was made for the mounting of a 4-in. (10.16-cm) span 60° delta wing on top of each of the models in three positions: wing trailing edge

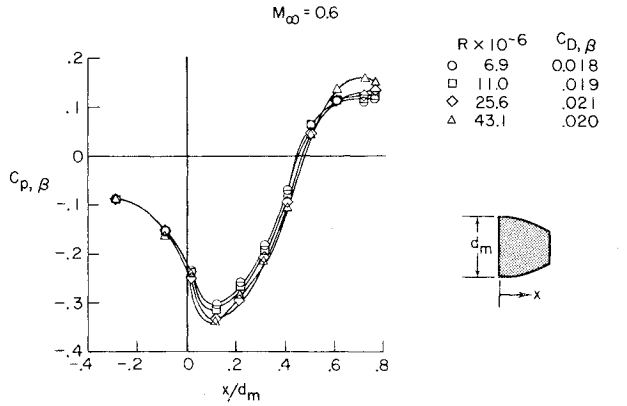

Fig. 5 Boattail pressure coefficient distributions for the circular arc boattail $l/d_m = 0.8$ at several Reynolds numbers.

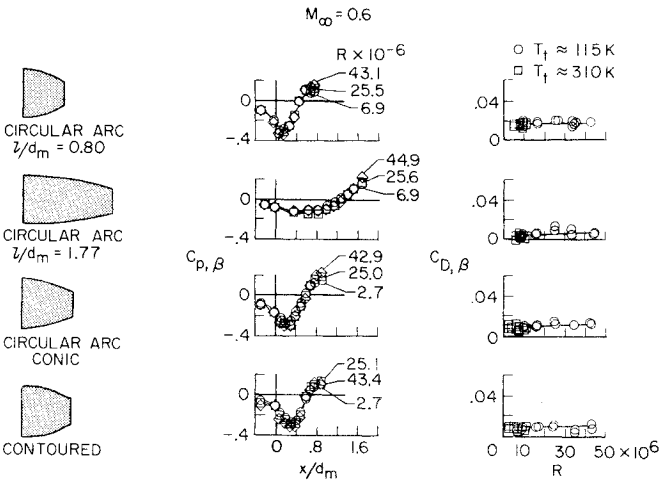

Fig. 6 Results of the investigation of the effect of Reynolds number on isolated boattails.

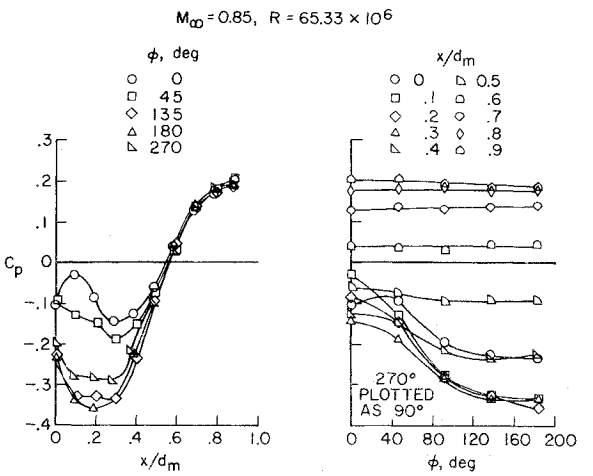

Fig. 7 Illustration of the effect of the presence of the wing on the boattail pressure coefficients for the circular arc-conic boattail.

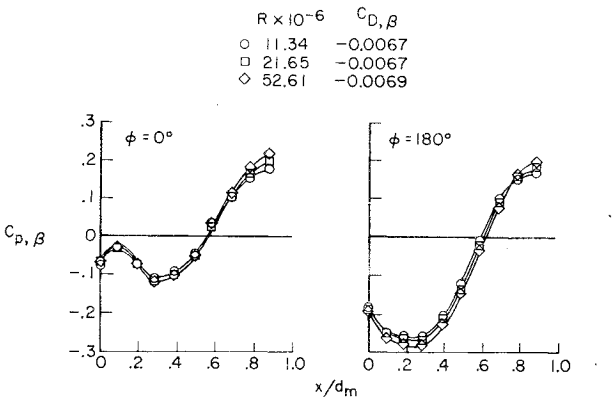

Fig. 8 Boattail pressure coefficient distributions for the circular arc-conic boattail (wing in the aft position) at several Reynolds numbers and $M = 0.6$.

0.05 d_m, 0.55 d_m, and 1.05 d_m forward of the start of the boattail (Fig. 3). The wing had a symmetric NACA 0003.9-65 airfoil section and was installed on the nacelle at 0° incidence. The lower surface of the wing was machined so that the chord line at the wing center line was tangent to the top of the nacelle.

Figure 4 is a photograph of one of the wing-body models mounted in the cryogenic tunnel. The tunnel has an octagonal test section 13.5 in. (34.29 cm) across the flats with slots at the corners of the octagon and is essentially a scale model of the Langley 16-ft transonic tunnel test section.[16] Tunnel blockage for the models of this investigation was slightly over 0.5%. Test medium for the cryogenic tunnel is nitrogen.

Results

Effects of Reynolds Number on Isolated Boattails

Boattail pressure coefficient distributions for the $l/d_m = 0.8$ circular arc boattail [8-in. (20.32-cm) model] obtained at four Reynolds numbers from about 7×10^6 to 43×10^6 at a Mach number of 0.6 are shown in Fig. 5. On the cylindrical portion of the model just upstream of the beginning of the boattail, the pressure coefficients at all four Reynolds numbers agree. However, as the flow expands around the shoulder of the boattail, the pressure coefficients at the different Reynolds numbers begin to spread apart such that the higher the Reynolds number the more negative the pressure coefficients in this expansion region. As the flow begins to recompress over the aft portion of the boattail, the trend is reversed; that is, the higher the Reynolds number the more positive the pressure coefficients. These two effects are compensating, and, as a result, the integrated boattail pressure drag coefficients are about the same for all four Reynolds numbers.

The result shown in Fig. 5 is typical of that found for all four boattail geometries tested. The pressure coefficient distributions for all four of these boattails show the same trends as discussed previously (Fig. 6). As Reynolds number is increased, the expansion pressure coefficients become more negative, whereas the recompression pressure coefficients become more positive. As a result, the integrated boattail pressure drag coefficients show essentially no change with Reynolds number. Similar trends in both pressure coefficients and pressure drag coefficients have been reported by Zonars et al.[17] and Lee.[18]

All data presented in Figs. 5 and 6 are for the short [8-in. (20.32-cm)] models at $M = 0.6$. Similar trends with Reynolds number both in pressure coefficients and pressure drag coefficients are observed for the long [16-in. (40.64-cm)] models. Also, data at $M = 0.9$ for both short and long models are similar.

Effects of Reynolds Number on Wing-Body Boattails

Boattail pressure coefficients for the circular arc-conic boattail at $M = 0.85$ and a Reynolds number of 65.33×10^6 are shown in Fig. 7. This figure has plots of boattail pressure coefficient as a function of x/d_m for the five rows of orifices and boattail pressure coefficient as a function of ϕ for the ten x/d_m stations. As can be seen, the presence of the wing results in a significant increase in the pressure level over about the first half of the boattail for at least half of its circumference. Similar, but not quite as large, effects were observed for the $l/d_m = 1.77$ circular arc boattail.

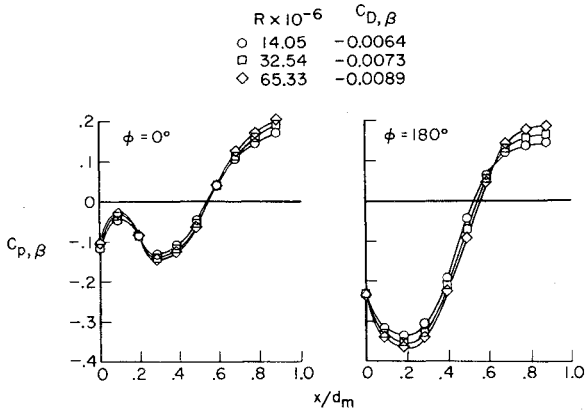

Fig. 9 Boattail pressure coefficient distributions for the circular arc-conic boattail (wing in the aft position) at several Reynolds numbers and $M = 0.85$.

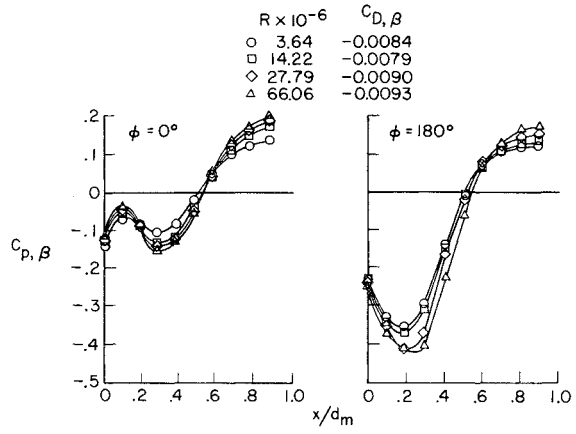

Fig. 10 Boattail pressure coefficient distributions for the circular arc-conic boattail (wing in the aft position) at several Reynolds numbers and $M = 0.9$.

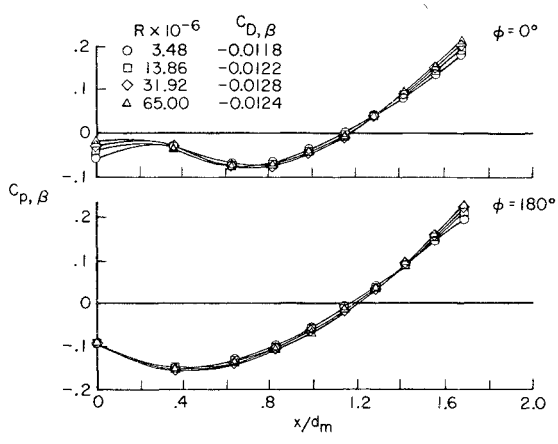

Fig. 11 Boattail pressure coefficient distributions for the circular arc boattail (wing in the aft position) at several Reynolds numbers and $M = 0.85$.

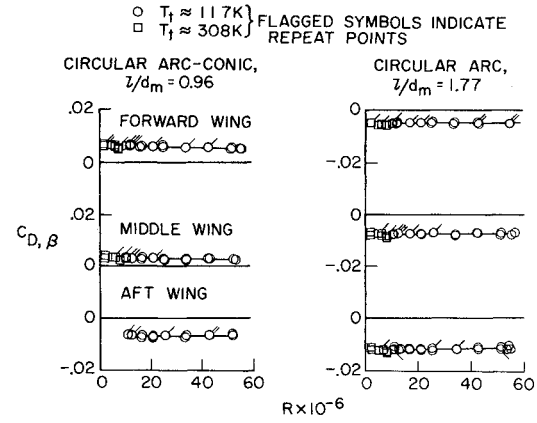

Fig. 12 Boattail pressure drag coefficients for both boattails and all three wing positions as a function of Reynolds number for $M = 0.6$.

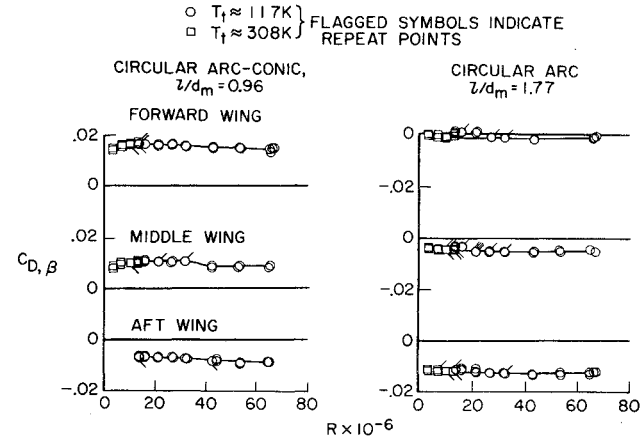

Fig. 13 Boattail pressure drag coefficients for both boattails and all three wing position as a function of Reynolds number for $M = 0.85$.

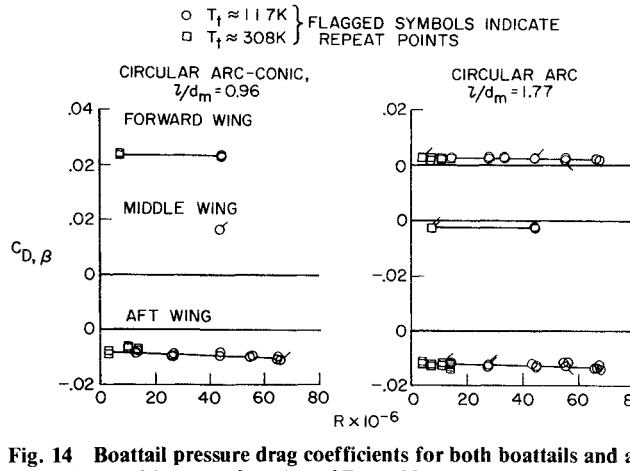

Fig. 14 Boattail pressure drag coefficients for both boattails and all three wing positions as a function of Reynolds number for $M = 0.9$.

Boattail pressure coefficient distributions for the circular arc-conic boattail with the wing in the aft position at several Reynolds number are shown in Figs. 8-10 for Mach numbers of 0.6, 0.85, and 0.9, respectively. Although it is apparent from Fig. 7 that the presence of the wing has large effects on the boattail pressure coefficients, it is also apparent from Figs. 8-10 that the trends with Reynolds number are the same as those found for the isolated boattails. That is, the pressure coefficients in the expansion region become more negative with increasing Reynolds number, whereas those in the recompression region become more positive. The resulting boattail drags also show little change with Reynolds number.

Similar statements can be made about the data for the $l/d_m = 1.77$ circular arc boattail. Typical results are shown in Fig. 11 for a Mach number of 0.85. The presence of the wing again results in an elevated pressure level over part of the boattail, and the trends of decreased expansion pressure coefficients and increased recompression pressure coefficients with increasing Reynolds number are exhibited. Also, the pressure drag coefficients are about the same for all Reynolds numbers.

Although not presented herein, the data for both boattails with the wing in the other two positions show that, as the wing was moved forward away from the boattail, the effect of the presence of the wing on the boattail pressure coefficients was lessened. However, the same trends with Reynolds number were observed.

Boattail pressure drag coefficients as a function of Reynolds number for both the circular arc-conic and circular arc boattails for all three wing positions and at Mach numbers of 0.6, 0.85, and 0.9 are shown in Figs. 12-14. For all combinations tested (not all wing positions were tested extensively at $M=0.9$), there is essentially no effect of Reynolds number on boattail pressure drag. These figures also show that the wing has a beneficial interference effect on the boattail pressure drag: the closer the trailing edge of the wing is to the start of the boattail, the lower the boattail pressure drag.

Concluding Remarks

The current assessment of the effects of Reynolds number on the pressure distributions on and the pressure drag of the boattails of two wing-body models has indicated several significant results. The general effect of increasing Reynolds number is to make the pressure coefficients in the expansion region of the boattail more negative and those in the recompression region more positive. These two effects are compensating, and, as a result, there is little or no effect of Reynolds number on the pressure drag of these boattails in an installed flowfield. These results are exactly the same as those previously reported for a series of isolated boattails. It would, therefore, seem that, based on the results of these two investigations, the large effects of Reynolds number observed in the previous NASA work were due to installed nozzle flowfield effects that cannot be duplicated simply. Further work must be done in order to isolate these effects.

References

[1]Chamberlin, R., "Flight Investigation of 24° Boattail Nozzle Drag at Varying Subsonic Flight Conditions," NASA TM X-2626, 1972.

[2]Chamberlin, R. and Blaha, B. J., "Flight and Wind Tunnel Investigation of the Effects of Reynolds Number on Installed Boattail Drag at Subsonic Speeds," NASA TM X-68162, 1973.

[3]Wilcox, F. A., "Comparison of Ground and Flight Test Results Using a Modified F-106B Aircraft," AIAA Paper 73-1305, Las Vegas, Nevada, Nov. 1973.

[4]Chamberlin, R., "Flight Reynolds Number Effects on Contoured Boattail Nozzle at Subsonic Speeds," NASA TM X-3053, 1974.

[5]Wilcox, F. A. and Chamberlin, R., "Reynolds Number Effects on Boattail Drag of Exhaust Nozzles from Wind Tunnel and Flight Tests," AGARD Paper 21, CP-150, 1975.

[6]Goodyer, M. J. and Kolgore, R. A., "The High Reynolds Number Cryogenic Wind Tunnel," *AIAA Journal*, Vol. 11, May 1973, pp. 613-619.

[7]Kolgore, R. A., Adcock, J. B., and Ray, E. J., "Flight Simulation Characteristics of the Langley High Reynolds Number Cryogenic Tunnel," *Journal of Aircraft*, Vol. 11, Oct. 1974, pp. 593-600.

[8]Ray, E. J., Kilgore, R. A., Adcock, J. B., and Davenport, Ed. E., "Test Results from the Langley High Reynolds Number Cryogenic Transonic Tunnel," *Journal of Aircraft*, Vol. 12, June 1975, pp. 539-544.

[9]Polhamus, E. C., Kilgore, R. A., Adcock, J. B., and Ray, E. J., "The Langley Cryogenic High Reynolds Number Wind-Tunnel Program," *Astronautics & Aeronautics*, Vol. 12, Oct. 1974, pp. 30-40.

[10]Kilgore, R. A., Goodyer, M. J., Adcock, J. B., and Davenport, E. E., "The Cryogenic Wind-Tunnel Concept for High Reynolds Number Testing," NASA TN D-7762, 1974.

[11]Kilgore, R. A., Adcock, J. B., and Ray, E. J., "Simulation of Flight Test Conditions in the Langley Pilot Transonic Cryogenic Tunnel," NASA TN D-7811, 1974.

[12]Ray, E. J., Kilgore, R. A., Adcock, J. B., and Davenport, E. E., "Analysis of Validation Tests of the Langley Pilot Transonic Cryogenic Tunnel," NASA TN D-7828, 1975.

[13]Reubush, D. E., "The Effect of Reynolds Number on Boattail Drag," *Journal of Aircraft*, Vol. 13, May 1976, pp. 334-337.

[14]Reubush, D. E., "Experimental Study of the Effectiveness of Cylindrical Plume Simulators for Predicting Jet-On Boattail Drag at Mach Numbers Up to 1.30," NASA TN D-7795, 1974.

[15]Cahn, M. S., "An Experimental Investigation of Sting-Support Effects on Drag and a Comparison With Jet Effects at Transonic Speeds," NACA Rept. 1353, 1958.

[16]Corson, B. W. Jr., Runckel, J. F., and Igoe, W. B., "Calibration of the Langley 16-Foot Transonic Tunnel With Test Section Air Removal," NASA TR R-423, 1974.

[17]Zonars, D., Laughrey, J. A., and Bowers, D. L., "Effects of Varying Reynolds Number and Boundary Layer Displacement Thickness on the External Flow Over Nozzle Boattails," *AGARD Specialists Meeting on Airframe/Propulsion Interference*, Sept. 1974.

[18]Lee, J.D., "An Experimental Study of Boattail Pressures at High Subsonic Mach Numbers and High Reynolds Numbers," AFSC/USAF ARL TR 75-0014, 1975.